The Parton Structure of Protons and Photons Measured at the ep Storage Ring HERA

D. Wegener*
Institute of Physics, University of Dortmund

1. Structure of the Proton

Starting with the pioneering experiment of the SLAC–MIT group [1] deep inelastic lepton proton scattering has provided a great amount of information on proton structure. The inclusive deep inelastic scattering process of electrons on protons is described by the Feynmangraph shown in fig.1. The kinematical variables can be derived from the four momenta of the leptons and the hadrons in the final state respectively:

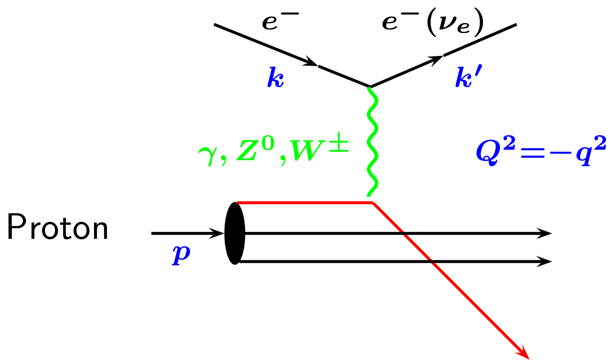

Figure 1. Kinematical variables in $ep \to e\,X$ reactions in leading order

$$s = (p+k)^2 \quad (1) \qquad Q^2 = -(k-k')^2 \quad (4)$$

$$y = \frac{q \cdot p}{k\,p} \quad (2) \qquad x = \frac{Q^2}{2\,p\,q} \quad (5)$$

$$W^2 = (q+p)^2 = Q^2\,(\frac{1}{x} - 1) \quad (3) \qquad Q^2 = s\,x \cdot y \quad (6)$$

Three of these variables are linear independent.The measurements at HERA increased the accessible range of Q^2 and x each by more than two orders of magnitude [2].

The cross section is given by the expression

$$\frac{d^2\sigma}{dx\,dQ^2} = \frac{2\pi\,\alpha^2}{x\,Q^4} \left\{ (1 + (1-y)^2)\,F_2\,(x,Q^2) - y^2\,F_L\,(x,Q^2) \right\} . \quad (7)$$

*representing the H1 and ZEUS collaboration, Paper presented at QNP 2000, Adelaide, February 21–25, 2000

In the framework of the quark–parton model [3] the structure functions depend only on the Bjorken variable x, they are related to the quark momentum distribution $q\,(x)$

$$F_2\,(x) = \sum e_i^2\, x \cdot q\,(x) \tag{8}$$

and the longitudinal structure function F_L is equal to zero, since quarks have spin 1/2.

QCD predicts a Q^2–dependence of the structure functions

$$F_2 = F_2\,(x, Q^2) \tag{9}$$ and $$F_L = F_L\,(x, Q^2) \neq 0 \tag{10}$$

due to gluon emission. Precise measurements of these structure functions constrain QCD in NLO. It is convenient for some analysis to introduce the ratio

$$R = \frac{F_L}{F_2 - F_L}\,. \tag{11}$$

In this case the cross section eq.(7) amounts to

$$\frac{d^2\sigma}{dx\, dQ^2} = \frac{2\pi\, \alpha^2}{x\, Q^4} \left\{ (1 + (1-y)^2) - \frac{y^2}{1 + 1/R} \right\} F_2\,(x, Q^2)\,. \tag{12}$$

The Q^2–dependence of $F_2\,(x, Q^2)$ is given by the DGLAP equation [4]

$$\frac{\partial}{\partial\, ln\, Q^2} \begin{pmatrix} q_i\,(x, Q^2) \\ g\,(x, Q^2) \end{pmatrix} = \frac{\alpha_s\,(Q^2)}{2\pi} \begin{pmatrix} P_{qq} & P_{qg} \\ P_{gq} & P_{gg} \end{pmatrix} \otimes \begin{pmatrix} q_i\,(x, Q^2) \\ g\,(x, Q^2) \end{pmatrix}. \tag{13}$$

The splitting functions follow from perturbative QCD. According to eq.(13) the gluon structure $g\,(x, Q^2)$ can be derived from the Q^2–dependence of the structure function. Hence measurements of $F_L\,(x,\, Q^2)$ allow to study the proton structure, moreover, they are an essential input to predictions of cross sections relevant for LHC experiments.

The kinematical variables of the inclusive scattering process $e\,p \to e\,X$ can be deduced in different ways from the final state particles detected by the 4π–spectrometers at HERA:

- from the scattered electron
- from the hadrons in the final state
- combining the two informations

The advantages are obvious. Most important is the possibility to perform systematic checks. Nowadays typical systematic errors are smaller than 3 %, if one choses the optimal method for the kinematical region studied. Note that for charged current reactions $e\,p \to \nu_e\, X$ only the hadron variables can be used to determine the kinematical variables.

1.1. Measurement of $F_2\,(x, Q^2)$

Typical results of the structure function $F_2\,(x, Q^2)$ at low x are shown in fig.2 [2]. Compared to the first HERA results the errors are reduced by a factor 2 to 3. The structure functions shown have been derived from the measured cross sections assuming $R = 0$ in eq.(12), the uncertainty in the lowest x bin due to this assumption amounts to 5 %–10 %, it is negligible at larger values of x. Good agreement with previous fixed target data, covering the region $x > 0.01$, is achieved on the few percent level. Unexpected for most was the steep rise at low x with decreasing x and the steep increase with Q^2 at fixed x (fig.2), which turns out to be due to gluon radiation by partons [5]. The data are in good agreement with NLO QCD fits for $Q^2 > 1\,\mathrm{GeV}$ (fig.3) [6], i.e. $p\,$QCD permits to describe the data. Note that Glück et al. [5] predicted this behavior before HERA started data taking. For $Q^2 < 0.3\,\mathrm{GeV}^2$ the data can be parametrized with the help of a Regge ansatz, successful in low p_t hadronic sections. The interval $0.3\,\mathrm{GeV}^2 < Q^2 < 1\,\mathrm{GeV}^2$ corresponds to a transition between low p_t physics, characterized by nonperturbative phenomena, and deep inelastic scattering treatable by perturbative QCD.

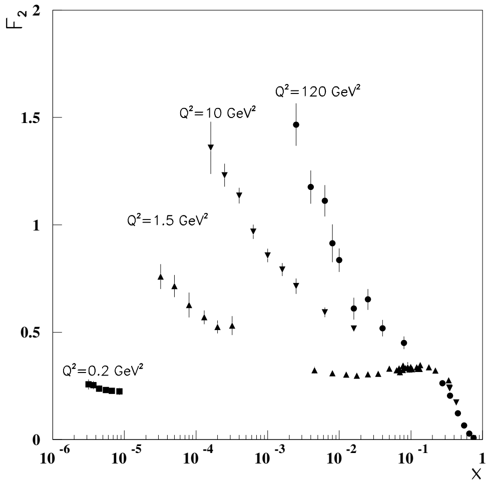

Figure 2. $F_2\,(x, Q^2)$ from HERA and fixed target experiments [2]

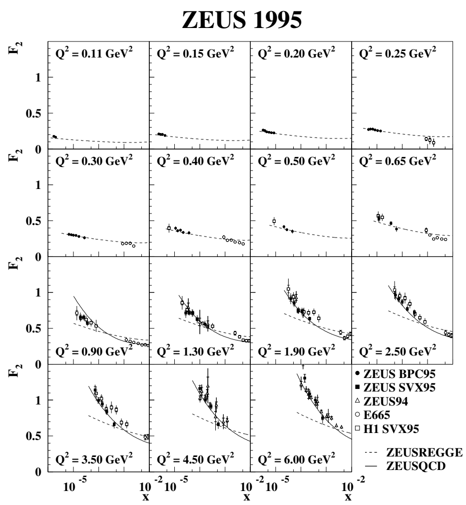

Figure 3. $F_2\,(x, Q^2)$ at small Q^2, compared to a QCD and a Regge fit [6]

Recently a high statistic sample became available at HERA for $Q^2 < 30\,000\,\mathrm{GeV}^2$ [7]. Extrapolating a NLO QCD fit, applied to low Q^2 data, to the new kinematical region of high Q^2, one observes excellent agreement as demonstrated by fig.4, where

$$\tilde{\sigma}\,(e\,p \to e\,X) = \frac{1}{1 + (1-y)^2}\,\frac{Q^4 x}{2\pi\,\alpha^2}\,\frac{d^2\sigma}{dx\,dQ^2} \tag{14}$$

is plotted as function of x for different Q^2 intervals. After the luminosity upgrade of HERA the valence quark distributions $u_v\,(x, Q^2)$ and $d_v\,(x, Q^2)$ can be determined separately from a combination of neutral and charged current inclusive ep scattering data. Thus the well known complications due to nuclear effects will be avoided which limits presently the precision achievable specifically at high x.

A QCD analysis of HERA and fixed target structure function data have been performed by Botje [8]. In fig.5 the valence–, sea–quark and gluon momentum distributions are shown for $Q^2 = 10\,\mathrm{GeV}^2$. At $Q^2 = 10\,\mathrm{GeV}^2$ the valence quark distributions peak at $x \approx 0.2$, while the sea–quark and the gluon distribution rise steeply with $x \to 0$. Note that the ratio d_v/u_v due to the influence of nuclear binding effects is hardly constrained by present data, it is even not clear if the ratio approaches a finite value in the limit $x \to 1$ [8].

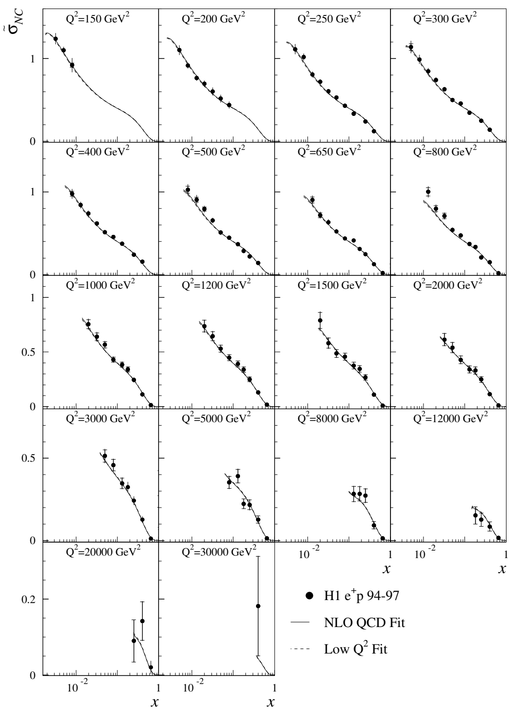

Figure 4. $F_2\,(x, Q^2)$ for large Q^2 compared to a NLO QCD–fit [7]

1.2. Structure function $F_L\,(x, Q^2)$

The longitudinal structure function $F_L\,(x, Q^2)$ is produced by radiative effects and, therefore, provides a sensitive test of perturbative QCD. As follows from eq.(7) F_L contributes to the measured cross section mainly in the limit $y \to 1$. Three methods presently are exploited to derive F_L from data. According to eq.(6) one can run at different *cms* energies or select events with initial state radiation thus varying y at fixed x, Q^2. The latter method is at present under study [9]. An indirect way exploits the y^2–factor in front of F_L (eq.(7)). At low y data are insensitive to F_L, therefore, in this region one determines $F_2\,(x, Q^2)$, fits the data by a pQCD ansatz, extrapolates them to high y and substracts this contribution. Another approach exploits the fact that at low y $\frac{\partial\,\tilde{\sigma}}{\partial\,ln\,y}$ depends linearly on $ln\,y$, while for the largest y F_L dominates the derivative. The results obtained [10] by these two methods are shown in fig.6, they are in good agreement with QCD predictions. Note that F_L is much smaller than F_2.

1.3. Charm contribution to F_2

The production of charmed particles is dominated by photon–gluon fusion (fig.7). The charm structure function of the proton is given by the expression

$$\frac{d^2\sigma}{dx\,dQ^2} = \frac{2\pi\,\alpha^2}{x\,Q^4}\,(1 + (1-y)^2)\,F_2^c\,(x, Q^2)\,, \qquad (15)$$

if the contribution of F_L^c is neglected. A further source of uncertainties follows from the fact that charmed particles are detected only in a limited region of phase space,

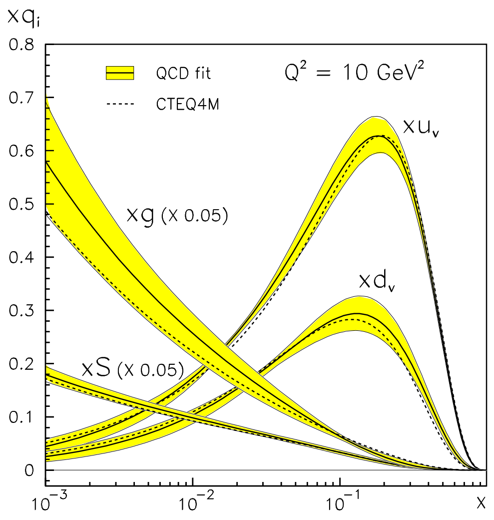

Figure 5. Valence quark (q_v), sea–quark (S) and gluon distribution derived from HERA and fixed target data [8]

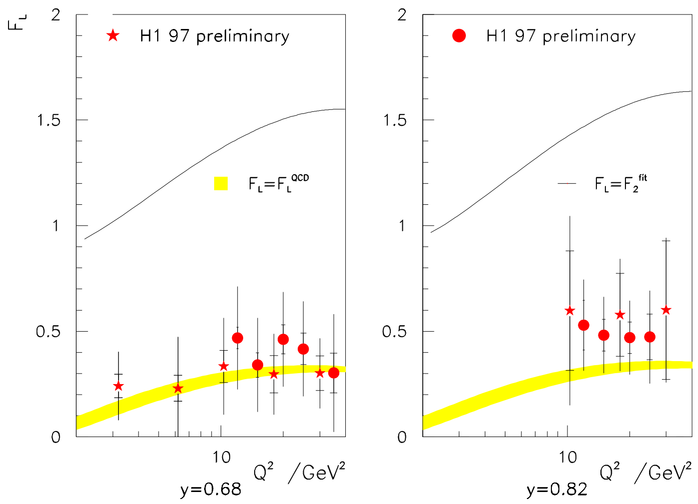

Figure 6. $F_L\,(x, Q^2)$ derived from HERA data [10]

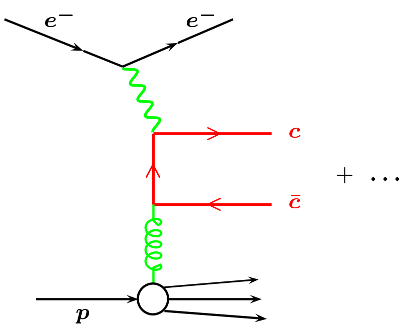

Figure 7. Charm production by photon–gluon fusion

hence model based extrapolations are necessary. In addition, the transition probability $c \to D^{*+}$–meson – the latter is used to tag charm production – is taken from e^+e^-–data. The measured cross section is shown in fig.8 [2]. F_2^c increases steeply with Q^2 and rises with decreasing x, a behavior characteristic for gluon produced particles. At high Q^2 and small x one finds $F_2^c/F_2 \approx 0.3$ [11]. The data are in good agreement with predictions from NLO perturbative QCD.

1.4. Gluon structure function $g\,(x, Q^2)$

Recently three methods have been used to measure the gluon structure function $g\,(x,\ Q^2)$. A global fit of the structure function $F_2\,(x,\ Q^2)$ exploiting eq.(13) allows to derive $g\,(x,\ Q^2)$ for $x < 0.01$. Photo– and electroproduction of D^*–mesons as well as 2 jet–production according to fig.7 can be used to determine $g\,(x,\ Q^2)$. Results of these studies are combined in fig.9. The theoretically expected gluon structure function is included [2]. The results of the different data sets agree with each other and coincide with the pQCD prediction. Clearly an extension of this analysis to higher x values ($x \approx 0.2$) is highly desirable, since gg–contributions dominate the Higgs production at LHC and values of the Bjorken variable $x \approx \sqrt{m_H^2/s}$ are of interest.

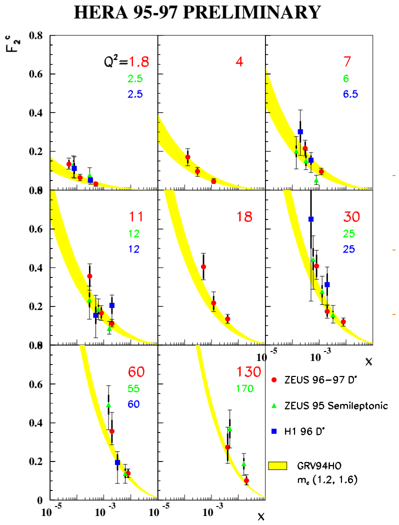

Figure 8. $F_2^c\,(x, Q^2)$ compared to QCD prediction

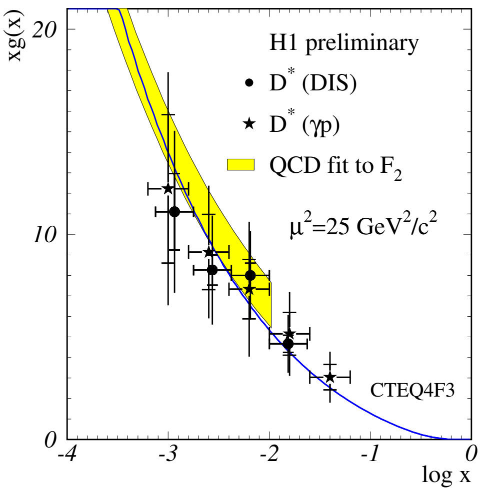

Figure 9. Gluon structure function $g\,(x, Q^2)$

2. Structure of the photon

The photon as the gauge boson of QED is assumed to be elementary, however, it is expected to have a hadronic structure due to quantum fluctuations. The leading order contribution is shown in fig.10. The cross section of processes where the photon enters the hard process directly ("direct photon") and those where it has a structure ("resolved photon") are of comparable size. In photoproduction ($Q^2 \to 0$) the hard scale is related to E_T^2, while in deep inelastic 2 jet–processes Q^2 and E_T^2 serve as hard scale. In the latter case the structure of the **virtual** photon should be resolvable if $E_T^2 \gg Q^2$. The parton momentum in the photon x_γ is related to the rapidity η and the transverse energy E_T of the jets

$$x_\gamma = \frac{\sum E_T^{jet}\, e^{-\eta_{jet}}}{2y \cdot E_e}\,. \tag{16}$$

The jet cross section depends on the parton distribution functions q_p, g_p of the proton, the partonic cross section of the hard scattering process $d\sigma/dt$ and the quark and gluon distribution functions $q_\gamma\,(x_\gamma,\, E_T^2)$, $\;g_\gamma\,(x_\gamma,\, E_T^2)$ of the photon. In fig.11 the measured jet cross section $d\sigma/dE_T^{jet}$ is compared to NLO QCD calculations [12]. Good agreement is observed in general, deviations for $\eta_{jet} < 0$ can be traced back to fragmentation not considered in the calculation.

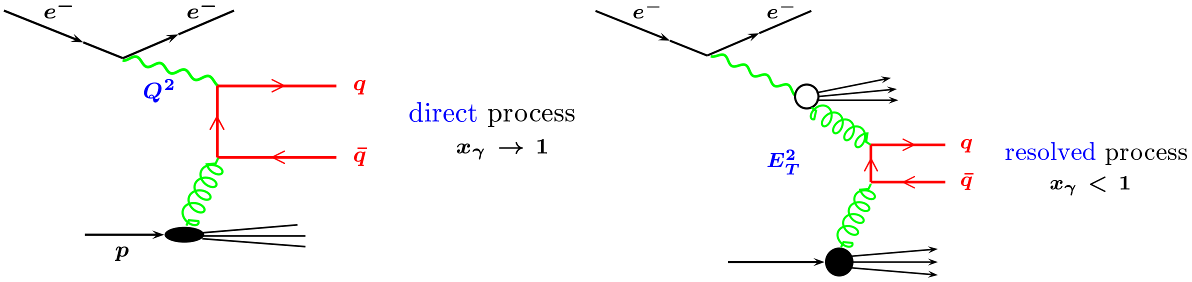

Figure 10. Contributions to photon structure in leading order

A comparison with a LO calculation allows to differentiate between the direct and the resolved contribution [13]. Since the quark distribution in the photon is known from $\gamma\gamma$–interactions, the gluon contribution can be extracted (fig.12). The photon emerges to have a gluon component – as expected in quantum field theories – which dominates at low x_γ, while the direct quark distribution peaks at large values of x_γ due to the direct photon component.

First results on the structure of the **virtual** photon became available recently, since measurements with $E_T^2 \gg Q^2$ have been performed [14]. The measured cross section as function of x_γ is shown in fig.13 for different intervals of E_T^2, Q^2. The data are compared to LO QCD calculations which consider both the direct and the resolved component of the virtual photon. While the direct component contributes to the full data set, the resolved is only observed for $Q^2 < E_T^2$ and vanishes for $Q^2 \approx E_T^2$ (fig.13) where only the single $\gamma^*\, q\bar{q}$–coupling contributes.

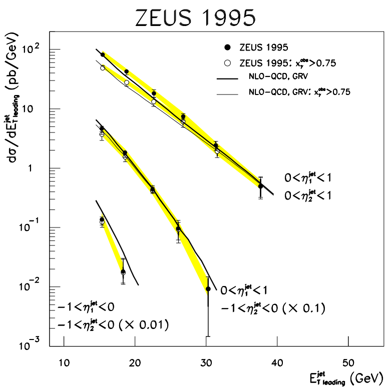

Figure 11. Jet production in $\gamma\, p$ reactions [12]

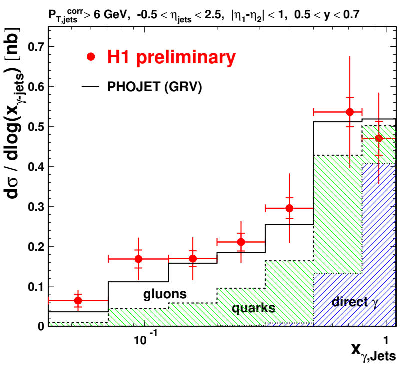

Figure 12. Jet production in $\gamma\, p$ reactions [13], the contribution of quarks and gluons are shown separately

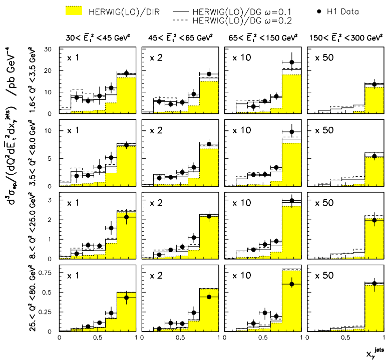

Figure 13. Jet production in $\gamma^* p$ reactions

3. Hard diffraction

3.1. Exclusive vector meson production

Recently the interest in exclusive vector meson electroproduction

$$e\,p \to e\,V p,\ V = \rho^o,\ \omega,\ \varphi,\ \psi,\ \Upsilon$$

was revived. While the classical VDM parametrizes the process by Pomeron exchange, nowadays the preferred QCD ansatz is 2 gluon exchange (fig.14). Which of the possible kinematical variables Q^2, M_V^2, t provides a hard scale has to be decided experimentally.

For real photons the total cross section and the exclusive ρ^o-, $\omega-$, φ–production cross section have an energy dependence characteristic for total hadron cross sections [15]. In the framework of VDM and using the optical theorem this observation can be explained by nonperturbative Pomeron exchange. On the other hand the exclusive $\psi-$ and $\Upsilon-$ photoproduction cross section increases much stronger with $W_{\gamma p}$ [16], hence M_ψ and M_Υ provide at high energies a hard scale.

The same trend of a steep increase of the cross section with $W_{\gamma^* p}$ is observed for the process $ep \to e\,\rho^o p$ if $Q^2 \gtrsim 3$ GeV^2 [2]. The study of its t–dependence leads to the same conclusion [18]. Different models have been proposed to explain the data. A nonperturbative ansatz is based on the Regge model and postulates a hard Pomeron with a Q^2–dependent intercept of the trajectory. Recently an ansatz based on $p\,$QCD has become popular (fig.14). The exchanged gluons carry different parton momenta with

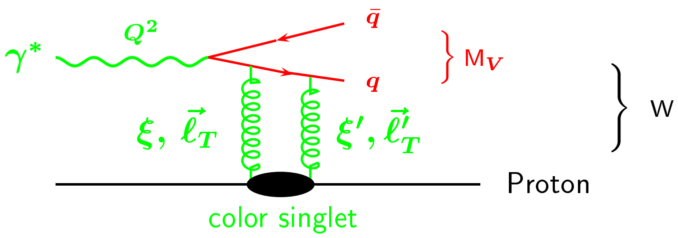

Figure 14. Deep inelastic exclusive vector meson production via 2 gluon exchange

$$\xi' - \xi = \frac{M_V^2 + Q^2}{W^2 + Q^2} = \delta\,\xi \tag{17}$$

For the Υ–meson the longitudinal momenta of the exchanged gluons differ considerably. Therefore, these processes allow to measure the so called skewed gluon distributions [19]. The cross section depends on the gluon structure function of the proton [20].

$$\frac{d\sigma}{dt}\,|_{t=0} \;\sim\; |\,\xi\, g(\xi,\, Q^2)\,|^2\ . \tag{18}$$

Further model assumptions concern the fragmentation of the $q\bar{q}$–state into vector mesons which either is parametrized by its wave function or via parton–hadron duality. The agreement between the theoretical prediction and the measured density matrix elements [17] for the process $e^- p \to e^- \rho^o p$ for 1 GeV^2 $< Q^2 <$ 60 GeV^2 is impressive (fig.15).

Note that s–channel helicity conservation (SCHC), which describes $\gamma\, p \rightarrow \rho^o\, p$ data with high precision, does not hold for electroproduction (fig.15, r^5_{oo}). Also the distributions of σ_L/σ_T, $\sigma\,(\gamma^* p \rightarrow \rho^o p)$ and $\frac{1}{<t>}$ as function of Q^2 accord with the model predictions [18] thus supporting the ansatz of fig.14.

Recently data for the deeply virtual Compton scattering (DVCS) became available [21,22]. Due to kinematics this process dominates in forward (proton) direction while in the backward region the QED Compton effect dominates (fig.17). Preliminary results (fig.16) agree with model predictions. The study of this process will reveal the cleanest information on skewed parton distributions, since the fragmentation $q\bar{q} \rightarrow \gamma$ can be treated theoretically without additional model assumptions.

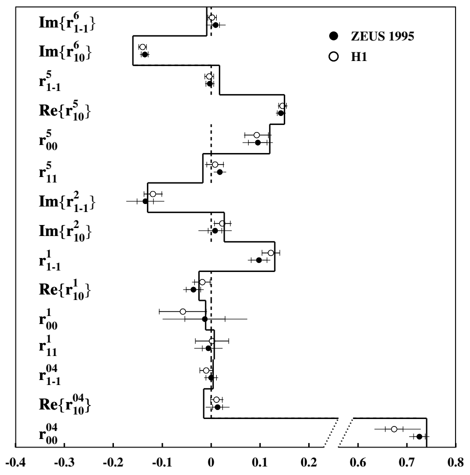

Figure 15. Density matrix elements for $\gamma^* p \rightarrow \rho^o p$ [17], - - - - SCHC

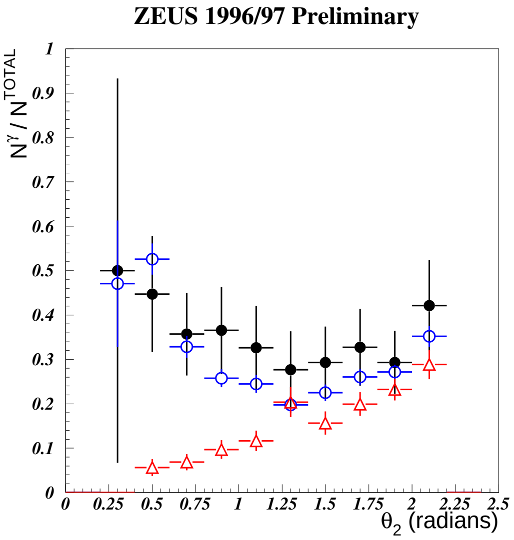

Figure 16. Rate of deeply virtual Compton scattering [21], Δ QED background, $\circ$ DVCS + QED

3.2. Inclusive hard diffractive scattering

In hadronic interactions diffractive processes account for $\sim$ 40 % of the total cross section. In these processes no quantum numbers are exchanged, they are of peripheral nature. Hadronic states with masses $M_x^2 < 0.2 \cdot W^2$ are excited coherently and the mass distribution peaks at low M_x^2 since $\frac{d\sigma}{d\,M_x^2} \sim M_x^{-2}$. In the framework of the Regge model Pomeron exchange is used to describe the data.

Unexpectedly a copious production of diffractive deep inelastic events, characterized by a large rapidity gap, was observed in $\sim$ 10 % of all deep inelastic events. Since Q^2 provides a hard scale, the study of these processes allows to determine the partonic content of the exchanged particle with vacuum quantum numbers. Hence one hopes to derive a connection between the fundamental degrees of freedom prevailing in soft physics (Regge trajectories) and those in hard processes (quarks and gluons). The kinematics of this process and the relevant kinematical variables are defined in fig.18. Experimentally diffractive events are either identified by a forward proton or neutron along the beam line or a rapidity gap separating target and current fragmentation region. The structure function is given by the expression

$$F_2^{D(3)}(x_{I\!P},\, Q^2,\, \beta) = \frac{\beta \cdot Q^4}{2\pi\,\alpha^2}\ \frac{1}{1+(1-y)^2}\ \frac{d^3\,\sigma_D}{dQ^2\,d\beta\,dx_{I\!P}}\,. \tag{19}$$

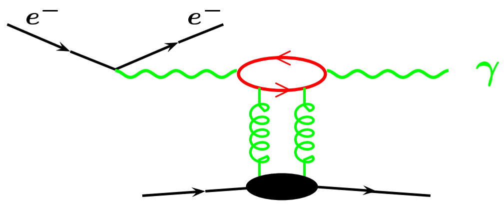

Figure 17. Deeply virtual Compton scattering via 2 gluon exchange

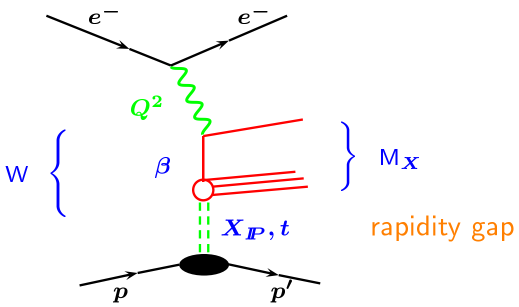

Figure 18. Kinematical variables of deep inelastic diffractive scattering

Contributions of the longitudinal structure function are neglected. Typically the structure function eq.(20) at fixed $x_{I\!P}$ turns out to be flat in β (fig.19) in strong contrast to the observation for protons (fig.2, 3) [23]. The Q^2–dependence is weak, at small β $F_2^{D(3)}$ rises with Q^2 while at large values of β it is more or less flat. These observations imply that the parton content of the system exchanged in hard diffractive events differs strongly from that of the proton. A QCD analysis of these dependencies therefore addresses the dynamical origin of the process. It starts from a parametrization of $F_2^{D(3)}$ and exploits the DGLAP evolution equations [25,26]. In contrast to the analysis of deep inelastic inclusive data no momentum sum rule exists, moreover, it is presumed that flavor symmetry of light quarks exists. The data can only be reproduced if a large and hard gluon component of the exchanged particle is assumed (fig.20). An independent check of this result is possible. If gluons are the dominant component, copious production of jets and D^*–mesons is expected (ch.1.3). Indeed, first results [27] with small statistics corroborate this conclusion.

Different approaches to describe the dynamics of hard diffractive scattering have been proposed. Phenomenological models start from the classical picture of diffraction mediated by Pomeron exchange. It turns out that the data enforce in addition to the hard Pomeron (ch.3.1) the exchange of a reggeon [26]. Especially interesting is a partonic ansatz, where a 2 gluon exchange mediates the interaction of the proton with a $q\bar{q}$ fluctuation of the virtual photon. Buchmüller et al. [24] arrived at a general description of deep inelastic scattering with a semiclassical approach. They assume that the photon fluctuates in a $q\bar{q}$–pair which interacts with the proton acting as a color source. If the $q\bar{q}$–pair in the final state is a color singlet the scattering is assumed to be diffractive otherwise it is treated as an ordinary deep inelastic event. This model reproduces with a minimal number of free parameters a large data set of hard diffractive and inclusive deep inelastic scattering for different x, $x_{I\!P}$, β and Q^2 values.

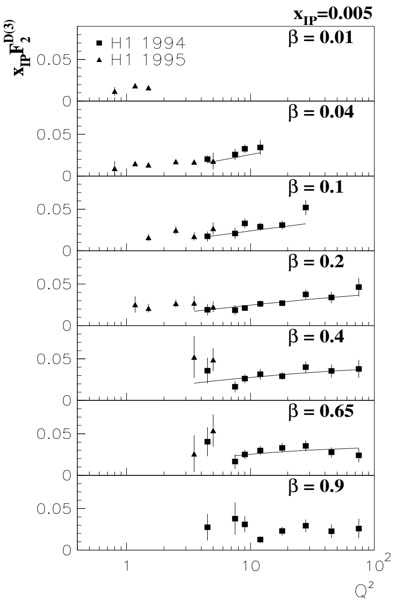

Figure 19. β–dependence of $F_2^{D(2)}(\beta, Q^2)$

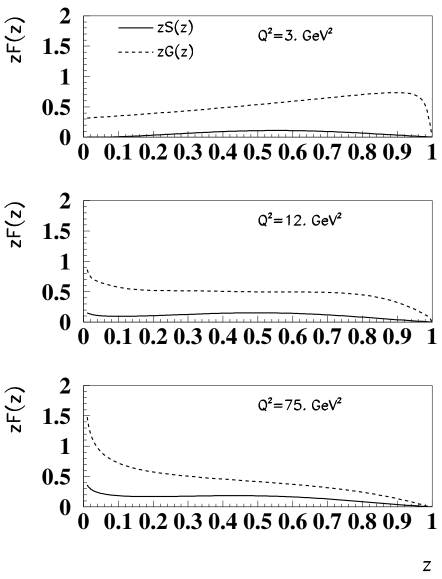

Figure 20. Quark and gluon contributions to $F_2^{D(3)}(z, Q^2, x_{I\!P})$ as derived with the DGLAP–equations [25,26]

4. Summary

The *ep*–storage ring HERA in recent years has become the leading factory for QCD studies. The kinematical region accessible to studies of the structure of the proton was increased at HERA by two orders of magnitude in x and Q^2. $p\,$QCD gives a precise description of the data. The most pronounced effect is the strong increase of the gluon component at low x. The photon structure has been studied, for the first time the gluon component of the photon was detected. Diffractive events in deep inelastic scattering turn out to be of great importance, the exchange particle is of gluonic nature and hard gluons are much more copious than for the proton.

The luminosity upgrade of HERA planned for 2001 will allow to reduce the statistical uncertainties which presently for some important problems are the limiting factor. It will, in addition, help to clarify if the “excess” of events at large x, Q^2 [28,29] and the excess of events with an isolated lepton and large missing p_t respectively are fluctuations or an indication of new physics.

Acknowledgement

It is a pleasure to thank my colleagues from H1 and ZEUS for providing the beautiful results and many interesting discussions. Dr. Thomas and colleagues I would like to thank for the invitation to this stimulating conference at such a nice place.

This work was supported by BMBF, Bonn, under contract number 7DO55P.

REFERENCES

1. E.D. Bloom et al., Phys. Rev. Lett. 23 (969) 930
   M. Breidenbach et al., Phys. Rev. Lett. 23 (969) 935
2. H. Abramowicz, A. Caldwell, Rev. Mod. Phys. 71 (1999) 1275
3. J.D. Bjorken, E.A. Paschos, Phys. Rev. 185 (1969) 1975
4. G. Altarelli, G. Parisi, Nucl. Phys. B126 (1977) 298
   V.N. Gribov, L.N. Lipatov, Sov. J. Phys. 15 (1972) 438, 675
5. M. Glück, E. Reya, A. Vogt, Z. Phys. C53 (1992) 127
6. J. Breitweg et al. (ZEUS), Eur. Phys. J. C7 (1999) 609
7. C. Adloff et al. (H1), Eur. Phys. J. C13 (2000) 609
8. M. Botje, DESY 99–038
9. C. Issever, PhD thesis, Dortmund 2000
10. H1 contributed paper 534, 29th Intern. Conf. High Energy Physics, Vancouver 1998
11. J. Breitweg et al. (ZEUS), Eur. Phys. J. C12 (2000) 35
12. J. Breitweg et al. (ZEUS), Eur. Phys. J. C11 (1999) 35
13. C. Adloff et al. (H1), DESY 00–035
14. C. Adloff et al. (H1), Eur. Phys. J. C13 (2000) 397
15. Particle Data Group, Eur. Phys. J. 3 (1998) 1
16. P. Merkel, PhD thesis, Hamburg 1999, DESY-THESIS–1999–030
17. J. Breitweg et al. (ZEUS), Eur. Phys. J. C12 (2000) 393
18. C. Adloff et al. (H1), Eur. Phys. J. C13 (2000) 371
19. P. Kroll, These proceedings
20. S.J. Brodsky, L. Frankfurt, J.F. Gunion, A.H. Müller, M. Strikmann, Phys. Rev. D50 (1994) 3134
21. ZEUS collaboration, Paper presented to Intern. EPS Conference on HEP, Tamparene 1999
22. R. Stamen, Talk DIS 2000, Liverpool 2000
23. J. Breitweg et al. (ZEUS), Eur. Phys. J. C6 (1999) 43
24. W. Buchmüller, DESY 99–076
    W. Buchmüller, T. Gehrmann, A. Hebecker, Nucl. Phys. B537 (1999) 477
25. T. Nichols, C. Royon, L. Schoeffel, A. Van Haeck, Note H1–02/99–567
26. C. Adloff et al. (H1), Z. Phys. C76 (1997) 613
27. C. Adloff et al. (H1), Contributed papers 157ag, 157ac to Intern. EPS Conference on HEP, Tamparene 1999
28. C. Adloff et al. (H1), Z. Phys. C74 (1997) 191
29. C. Adloff et al. (H1), Eur. Phys. J. C5 (1998) 575